Ionics (2015) 21:2309–2317
DOI 10.1007/s11581-015-1423-1

ORIGINAL PAPER

High energy density asymmetric supercapacitors based on polyaniline nanotubes and tungsten trioxide rods

Kanjun Sun[1] **· Hui Peng**[2] **· Jingjing Mu**[2] **·**
Guofu Ma[2] **· Guohu Zhao**[1] **· Ziqiang Lei**[2]

Received: 6 December 2014 / Revised: 16 March 2015 / Accepted: 16 March 2015 / Published online: 14 April 2015

Abstract A high energy density asymmetric supercapacitor (ASC) is assembled utilizing polyaniline (PANI) nanotubes as the positive electrode and tungsten trioxide (WO_3) rods as the negative electrode. The PANI nanotubes are synthesized via a simple chemical template-free method in the presence of D-tartaric acid as the dopant, and ammonium persulfate as the oxidant, and the WO_3 rods are synthesized via a simple hydrothermal process in the presence of sodium carboxymethyl cellulose as a template. The PANI//WO_3 ASC device operates with a voltage of 2.0 V and achieved a remarkable specific capacitance of 151 F g^{-1} at a charge/discharge current density of 0.25 A g^{-1} and a high energy density of 41.9 Wh kg^{-1} at a power density of 261 W kg^{-1}. Furthermore, the device showed an excellent charge/discharge cycling performance in 1 M H_2SO_4 electrolyte, with capacitance retention of 71 % after 10,000 cycles. The high performance of the supercapacitor is due to the unique structure of the electrode materials which can provide high electrode/electrolyte contact area and make electrochemical reaction quickly.

Keywords Capacitors · Charging-discharging · Electrodes · Material preparation · Electrochemical characterizations

✉ Kanjun Sun
sunkj@lzcu.edu.cn

✉ Guofu Ma
magf@nwnu.edu.cn

[1] College of Chemistry and Environmental Science, Lanzhou City University, Lanzhou 730070, China

[2] Key Laboratory of Eco-Environment-Related Polymer Materials of Ministry of Education, Key Laboratory of Polymer Materials of Gansu Province, College of Chemistry and Chemical Engineering, Northwest Normal University, Lanzhou 730070, China

Introduction

Supercapacitors have received increasing attention as a promising energy storage device due to their high power density and exceptionally long cycle life [1, 2]. However, compared to commercial lithium ion and lithium polymer batteries, supercapacitors still present a drawback low energy density [3]. According to the equation of energy density (E=0.5CV^2), the energy density of supercapacitors can be improved by development of new electrode materials with wide operating voltage (V) and high specific capacitance (C) or using electrolyte with wide operating voltage [4]. The key to increasing the specific capacitance of electrode materials is to improve the microstructures where bulk redox reactions can occur both rapidly and reversibly, while minimizing ohmic losses through the electrode/current collectors [3, 5]. The operating voltage of organic electrolytes in supercapacitors can be up to 2.5 V [6]; however, they can make safety risks because of the flammability. On the other hand, the organic electrolyte has low ionic conductivity due to the larger molecule sizes, which can influence specific capacitance of the electrode. Conversely, supercapacitor utilizing aqueous electrolyte may display higher capacitance and higher power density than those with organic electrolytes, due to its high ionic conductivity [7].

Asymmetric supercapacitors (ASCs) are supercapacitors based on two different electrode materials to exhibit two different potential windows in the same electrolyte [8]. Therefore, this is an effective approach for extending the operating voltage window. For traditional asymmetric supercapacitor, one electrode is based on redox reaction pseudocapacitance electrode, and the other one is mostly based on electric double-layer carbon-based electrode. Intensive efforts have been devoted to explore various ASC systems, such as MnO_2//graphene [9], activated carbon//MoO_3 [10], CoO@Polypyrrole//activated carbon [11], and β-$Ni(OH)_2$//activated carbon [12]. The capacitance of an ASC is decided by both electrodes, as defined by the formula: $1/C_{cell}=1/C_{+} + 1/C_{-}$, where C_{cell} is an ASC capacitance, C_{+} and C_{-} are the capacitances of the positive and the negative electrodes [3]. As is well-known, the ASC devices are often use carbon materials as electrode materials; it largely restricts the improvement of energy density due to the unsatisfactory capacitive performance of those materials. However, it was found that the ASCs based on pseudocapacitance in both electrodes can be enhancing the capacitance and energy density, because these materials usually have a large specific capacity [8, 13–16]. Zou et al. assembled an ASC using WO_3/PANI as negative and PANI as positive electrodes over voltage range of 1.2 V which displays an energy density of 9.72 Wh kg^{-1} at the power density of 53 W kg^{-1} [15]. Xiao et al. fabricated an ASC using WO_{3-x}/MoO_{3-x} core/shell nanowires on carbon fabrics as negative electrodes and PANI as positive electrodes, which exhibited a high areal capacitance and high rate capability [16]. Despite these tremendous achievements, the drawbacks of these ASCs displayed the complex process of the electrode material synthetic route. Therefore, developing the ease of synthesis and low-cost ASCs with high energy density is still challenging.

Among all kinds of electrode materals for supercapacitors, polyaniline (PANI) has been most actively investigated due to its low cost, high specific capacity, and high conductivity [17]. In order to improve the physical and chemical properties of PANI, it is usually through the preparation of microstructure of PANI or copolymerization with other monomer preparation of PANI copolymer with nanostructure [18–20]. Transition metal oxides with nanostructure also show high specific capacity toward supercapacitors [21]. Typically, tungsten trioxide is an n-type semiconductor with different crystal structures that provide a suitable structure for intercalation of small H^+ cations, which provoke interesting energy storage properties [22–25]. In this work, we focused on enhancing the energy density of ASC based on pseudocapacitance in both electrodes, which is using polyaniline (PANI) nanotubes as a positive electrode and WO_3 rods as a negative electrode in 1 M H_2SO_4 aqueous electrolyte. Based on the difference of working potential window and high specific capacity between PANI and WO_3, the hybrid nanostructure ASCs (PANI//WO_3) operates with a voltage of 2.0 V and achieved a high energy density of 41.9 Wh kg^{-1} at a power density of 261 W kg^{-1}. In addition, the device showed an excellent cycling performance.

Experimental

Materials

Aniline monomer (Shanghai Chemical Works, China) was distilled under reduced pressure. D-tartaric acid (D-TA, Shanghai Chemical Works, China), ammonium persulfate (APS, Tianjin Damao Chemical Co., China), sodium tungstate dihydrate ($Na_2WO_4 \cdot 2H_2O$, Shanghai Chemical Works, China), sodium carboxymethyl cellulose (CMC, Tianjin Yuanli Chemical Co., China) were used as received. All solutions were prepared in deionized water. All chemical reagents were in analytical grade.

Synthesis of PANI nanotubes

The synthesis procedure of PANI nanotubes is similar to our lab previously reported [26]. In brief, aniline monomer (2 mmol) and D-tartaric acid (2 mmol) were dissolved in 10 mL of deionized water with magnetic stirring for 20 min at room temperature. After that, the resulting solution was cooled to below 5 °C in an ice bath, and an aqueous solution of APS (2 mmol in 5 mL of deionized water) cooled in advance was added drop-by-drop into the above solution. The mixtures were polymerized for 10 h without stirring at below 5 °C. The resulting precipitates were washed several times with deionized water and ethanol, respectively. Finally, the products were dried at 60 °C for 12 h to obtain a dark green powder.

Synthesis of WO_3 rods

The WO_3 rods were synthesized as follows: 0.825 g sodium tungstate dihydrate was dissolved in 20 mL (1 mg mL^{-1}) sodium carboxymethyl cellulose aqueous solution at ambient temperature. After stirring for 20 min approximately, 2 M HCl was added into the above solution mixture drop-by-drop under stirring to adjust the pH value to 2. Finally, the solution was transferred into a 100-mL Teflon-lined stainless steel autoclave and heated at 180 °C for 24 h. After cooling to room temperature naturally, the resulting precipitates of WO_3 were collected by filtration, washed with distilled water and absolute ethanol for several times to remove the residue of reactants, and then dried in vacuum at 60 °C for 12 h.

Characterizations

The as-prepared electrode materials were characterized by scanning electron microscopy (SEM, JSM-6701 F, Japan) at an accelerating voltage of 5.0 kV. The structure of the samples was characterized by a transmission electron microscopy (TEM, Tecnai G^2 F20 S-TWIN, USA). X-ray diffraction (XRD) of samples was performed on a diffractometer (D/Max-2400, Rigaku) advance instrument using Cu-Kα radiation (k=1.5418 Å) at 40 kV, 100 mA. The 2θ range used in the measurements was from 5 to 80°.

Electrochemical measurements

A typical three-electrode test cells in electrolyte were used for electrochemical measurement on CHI660D (Chenghua, Shanghai China) electrochemical working station. The working electrode used a glassy carbon electrode with a diameter of 5 mm. The reference electrode and counter electrode were saturated calomel electrode (SCE) and platinum electrode, respectively. The fabrication of the working electrodes refers to the literature [26]. Four micrograms of electroactive material was ultrasonically dispersed in 0.4 mL of Nafion (0.25 wt%). The above suspension of 8 mL was dropped onto the glassy carbon electrode using a pipet gun and dried at room temperature.

The gravimetric capacitance from galvanostatic charge/discharge was calculated by using the formula of $C_s = I\Delta t/(m\Delta V)$ for the three-electrode system, while, $C_s = 4I\Delta t/(m\Delta V)$ for the two-electrode cells, where I is the constant current (A) and m is the mass (g) of electrode material (for the two-electrode cells, m is the total mass of positive and negative electrodes), Δt the discharge time, and ΔV the voltage change during the discharge process.

Fabrication of asymmetric supercapacitor devices

Asymmetric supercapacitor devices were assembled with PANI nanotubes as the positive electrode and WO_3 rods as the negative electrode. The working electrode was prepared by mixing the electroactive material with polyvinylidene fluoride (PVDF) and carbon black (8:1:1) in N-methyl-2-pyrrolidone (NMP) until homogeneous slurry. The slurry was coated on carbon plate (99.99 %) with a working area of 1.0 cm^2, and the electrodes were dried at 120 °C for 12 h. The mass of PANI and WO_3 is loaded 3.4 and 4.6 mg, respectively. The electrodes were separated by a thin polypropylene.

The specific energy density (E, Wh kg^{-1}) and power density (P, W kg^{-1}) for a asymmetric supercapacitor cell can be calculated using the following equations: $E = 1/2CV^2$ and $P = E/t$, where C is the specific capacitance of supercapacitor cell, V is the voltage change during the discharge process after IR drop in V-t curve, and t is the discharge time.

Results and discussions

Morphology and structure of the PANI nanotubes and WO_3 rods

PANI nanotubes were synthesized via a simple chemical template-free method in the presence of D-tartaric acid as the dopant, and ammonium persulfate as the oxidant. Typical morphology and structure of the as-synthesized PANI nanotubes are given in Fig. 1. Figure 1a, b gives the images of as-synthesized PANI that exhibit nanotube morphology on a different magnification. As can be seen, the PANI products take on noteworthy nanotube shape, and the high magnification (Fig. 1b) illustrates that they are hollow structures. The diameter of the nanotubes is about 200 nm, and the wall thickness is about 50 nm. In addition, the external surface of these nanotubes is seen to be relatively rough and decorated by some PANI nanoparticles. This interesting structure of PANI nanotubes was further characterized by TEM. It is very obvious that the product of PANI nanotubes shows the nanotube structure (Fig. 1c, d), which is in agreement with the result of the SEM. This unique nanotubular structure can be providing a high electrode/electrolyte contact area and short ion diffusion path [26]. The XRD pattern of PANI nanotubes is shown in Fig. 1e. It can be seen that the PANI nanotubes have a primary characteristic peak at 20.3° attributed to the alternating distance between layers of polymer chains [27]. The FT-IR spectrum of PANI is shown in Fig. 1f. The peaks at 1570 and 1482 cm^{-1} are consistent with quinoid and benzene rings, respectively. The ones at 1300 and 1242 cm^{-1} are attributed to the C–N and C=N stretching vibrations of an aromatic amine. The peak at 1119 and 808 cm^{-1} is assigned to the aromatic C–H inplane and the out of plane deformation of C–H in the 1,4-disubstituted benzene ring, respectively [18, 28].

Figure 2a, b gives the SEM images of WO_3 that exhibit rod morphology on a different magnification. At a low magnification (Fig. 2a) for an overview, the WO_3 nanostructures are mainly rods with a random arrangement, and at high magnification (Fig. 2b), they exhibit clearly that the diameter of the nanorod is approximately 100 nm and the length is about 1 μm. The TEM and HRTEM images (Fig. 2c) show that WO_3 nanorod has a tunnel structure. The lattice spacing of 0.382 nm corresponds to the d-spacing of (001) planes [29]. The phase purity and crystal structure of the WO_3 rods were confirmed by XRD. As shown in Fig. 2d, all the diffraction peaks can be exclusively indexed to a hexagonal tungsten trioxide crystalline phase (h-WO_3, JCPDS No. 33-1387) [29], and no other impurities are observed from the XRD pattern. The strong and sharp diffraction peaks indicate good crystallinity of the as-synthesized products. Furthermore, hexagonal phase h-WO_3 has a unique tunnel structure, which can serve as an ion channel and quickly accelerating the electrochemical reaction rate [30].

Electrochemical properties of the PANI nanotubes and WO_3 rods

The electrochemical studies for the PANI nanotubes and WO_3 rods were first performed in a three-electrode cell using aqueous 1 M H_2SO_4 electrolyte (Fig. 3). Figure 3a, b shows the CV curves of PANI nanotubes positive electrode and WO_3 rods negative electrode at different scan rates, respectively. The

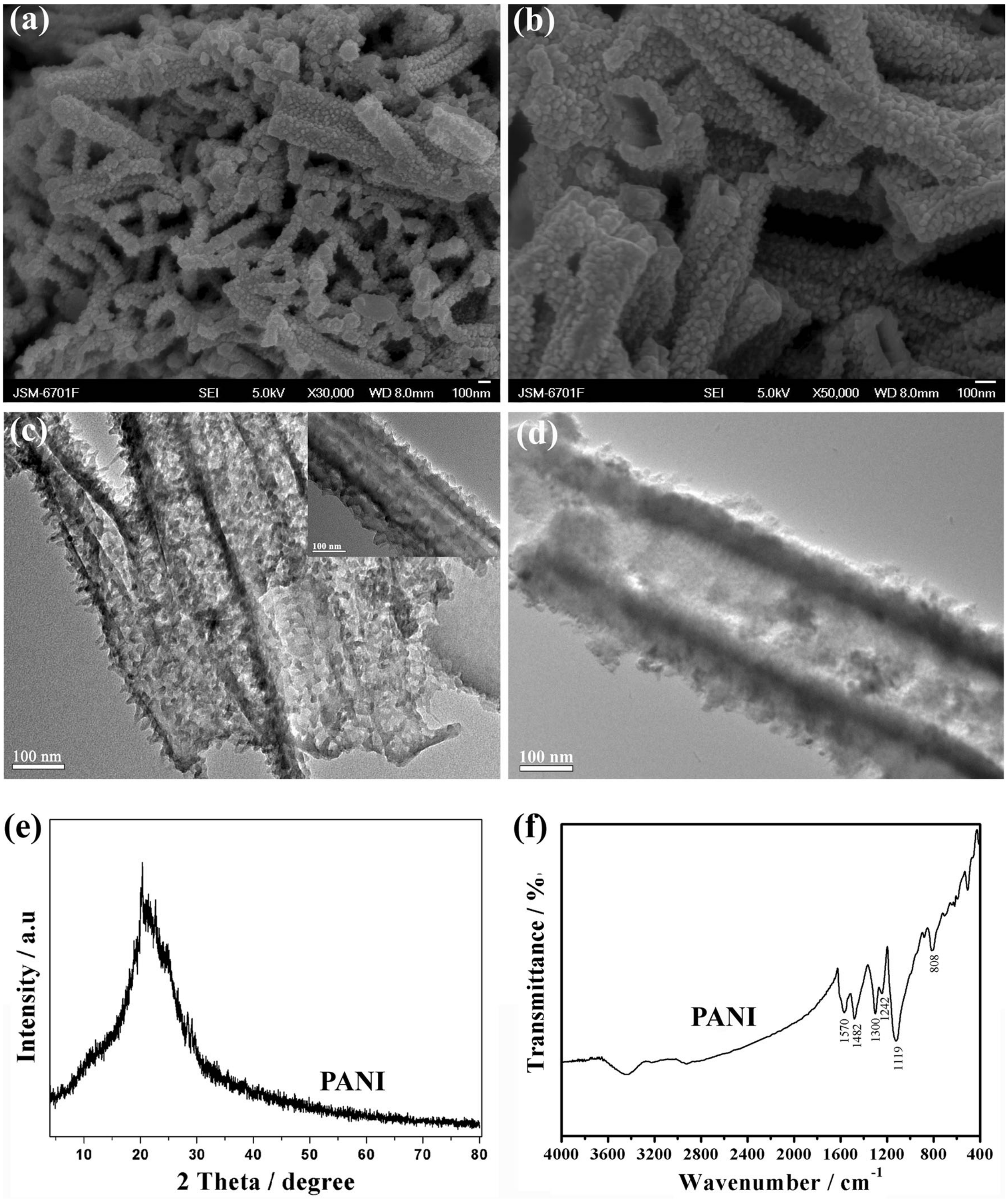

Fig. 1 **a**, **b** SEM images of as-synthesized PANI exhibit nanotubes morphology on a different magnification; **c**, **d** TEM images of PANI nanotubes; **e** XRD pattern of PANI nanotubes; **f** FT-IR spectra of PANI nanotubes

PANI nanotubes CV curves at different scan rates exhibited a near-rectangular shape with pseudocapacitance characteristics (Fig. 3a), and the typical redox peaks can clearly be found on the CV curves in the potential window of −0.2 to 0.8 V. The PANI have typical redox peaks: the first couple of peaks (about 0.21 V/0.10 V) are attributed to the redox transition of PANI between a semiconducting state (leucoemeraldine form) and a conducting state (polaronicemeraldine form); the peaks at 0.47/0.44, 0.55/0.53, and 0.76/0.70 V are ascribed to the benzo/hydroquinone (BQ/HQ), *p*-aminophenol/benzoquinoneimine (PAP/QI) redox pair and formation/reduction of bipolaronic pernigraniline and protonated quinonediimine, respectively [31]. Figure 3b shows the CV curves of WO_3 rod electrode at different scan rates in the potential window of −0.7 to 0 V with the electrolyte of 1 M H_2SO_4. The CV curves with the semirectangular and a hump shaped at different scan rates indicating pseudocapacitance is generated, in which process is in accordance with

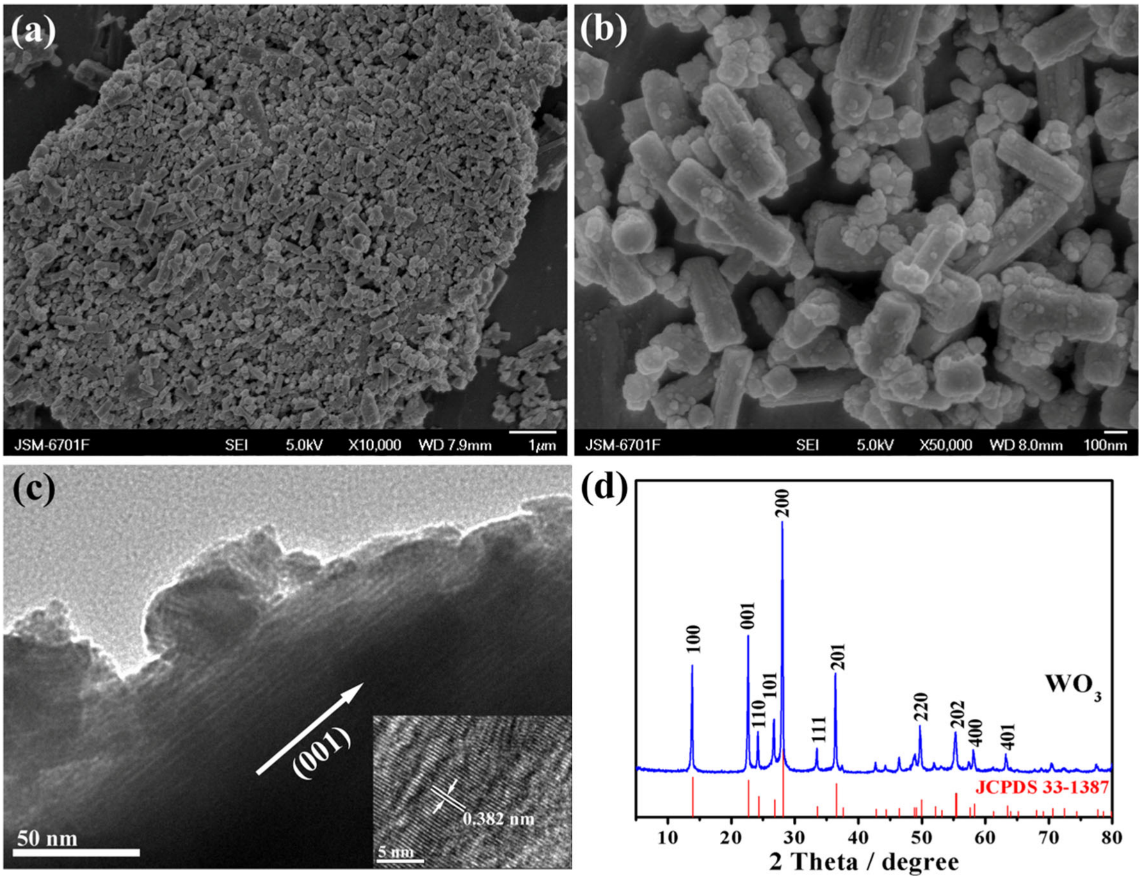

Fig. 2 **a**, **b** SEM images of as-synthesized WO_3 exhibits rod morphology on a different magnification; **c** TEM images of WO_3 rods (the *inset* shows the HRTEM images of WO_3 rods); **d** XRD pattern of WO_3 rods

intercalation/deintercalation of the H^+ into (out from) the WO_3 [32]: $WO_3 + xH^+ + xe^- \leftrightarrow H_xWO_3$. It is observed that CV curve area and the peak current rapidly increase with the increase of the scan rate. Moreover, CV curve shape had no obvious change even under the high scan rate. The result reveals that the WO_3 electrode has the reversible redox processes and good rate ability. Galvanostatic charge/discharge curves of PANI nanotubes positive electrode and WO_3 rods negative electrode that are collected at different current densities are shown in Fig 3c, d, respectively. All curves exhibited a symmetrical triangle shape, suggesting a good reversibility during the charge/discharge processes. The corresponding specific capacitances are calculated from galvanostatic charge/discharge curves and shown in Fig. 3e, f. The specific capacitance value of the PANI nanotubes is calculated as high as 541 F g^{-1} at current density of 1 A g^{-1}. Even at a current density as high as 10 A g^{-1}, the specific capacitance can still achieve to 391 F g^{-1}, which remains approximate to 72 % of the initial specific capacitance (Fig. 3e). The WO_3 rods also exhibit high specific capacitances of 573 and 311 F g^{-1} at a current density of 1 and 10 A g^{-1}, respectively. The PANI nanotube materials present a high capacitance that may attribute to unique nanotubular structure, which can be providing a high electrode/electrolyte contact area and short ion diffusion path. For hexagonal WO_3 rods (*h*-WO3), the electrons and ions in the electrolyte can fully insert and emerge in the electrode material at low current density because it has tunnel structure [30, 33], which led to the WO_3 rod electrode materials with high specific capacitance.

Considering high capacitance of the redox characteristics of PANI nanotubes and WO_3 rods, an asymmetric supercapacitor was fabricated using these materials as the positive and negative electrodes, respectively. The PANI was performed within a potential window of −0.2 to 0.8 V (vs SCE), while WO_3 electrode was measured within a potential window of −0.7 to 0 V (vs SCE) at a scan rate of 10 mV s^{-1} in 1 M H_2SO_4 electrolyte (Fig. 4a). Therefore, it is expected that the operating cell voltage as the sum of the potential range of PANI and WO_3, and it can be extended to 1.5 V when they are assembled into ASCs. However, since Zhang et al. [13] fabricated the asymmetric supercapacitor, RGO-RuO_2//RGO-PANI exhibited broad redox peaks that appeared on the CV curves between the −0.5 and 0.5 V, which are resulting from the reversible oxidation and reduction of PANI. Therefore, considering the reversible oxidation and reduction of PANI and the optimization of voltage window, the electrochemical

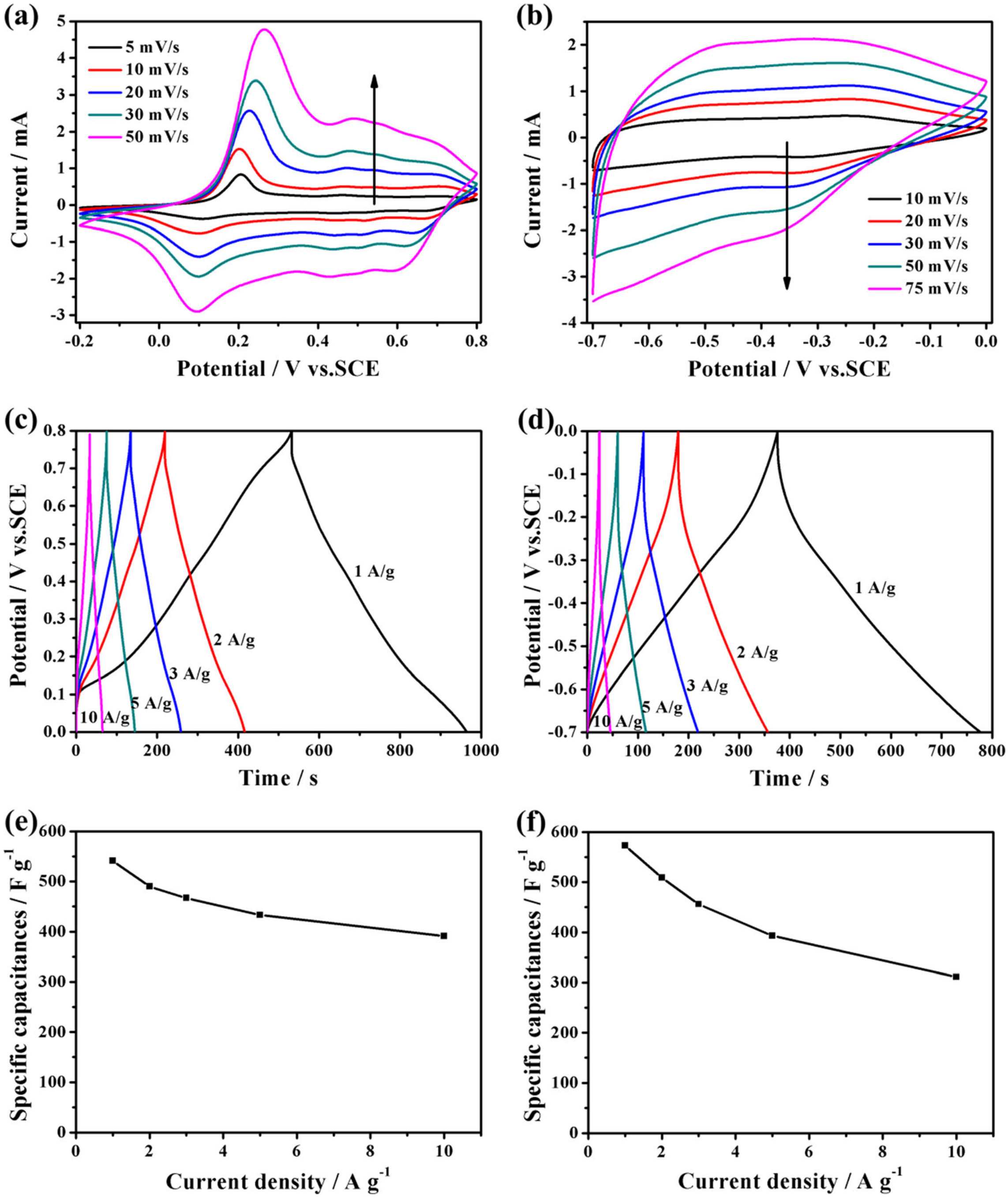

Fig. 3 **a**, **b** CV plots of the PANI and WO_3 electrodes at various scan rates performed in three electrode cell in 1 M H_2SO_4 electrolyte, respectively; **c**, **d** galvanostatic charge/discharge curves of PANI and WO_3 electrodes at different current densities performed in three electrode cell, respectively; **e**, **f** specific capacitance of the PANI and WO_3 electrodes at different current densities, respectively

measurements of the PANI//WO_3 asymmetric supercapacitor is performed in the voltage range of −0.5~1.5 V (Fig. 4b).

As for a supercapacitor, the charge balance will follow the relationship $q_+=q_-$, the stored charges are proportional to the specific capacitance (C), the voltage window (ΔE) and the mass (m) of the electrode following equation: $q=C\times\Delta E\times m$ [34]. Thus, $m^+/m^-=C_-\times\Delta E- \ / \ C_+\times\Delta E_+$, the mass ratio of $m_{(PANI)}/m_{(WO3)}$ was estimated to be 0.74 from the specific capacitance calculated from their galvanostatic charge/discharge curves. Figure 4b shows the CV curves of the PANI//WO_3 asymmetric cell measured at various scan rates of 5~50 mV s^{-1} between −0.5 and 1.5 V. These CV curves exhibit distorted shape indicating that pseudocapacitance is generated in asymmetric cell. To further evaluate the performance of asymmetric cell, we measured galvanostatic charge/discharge curves at various current densities (Fig. 4c). The

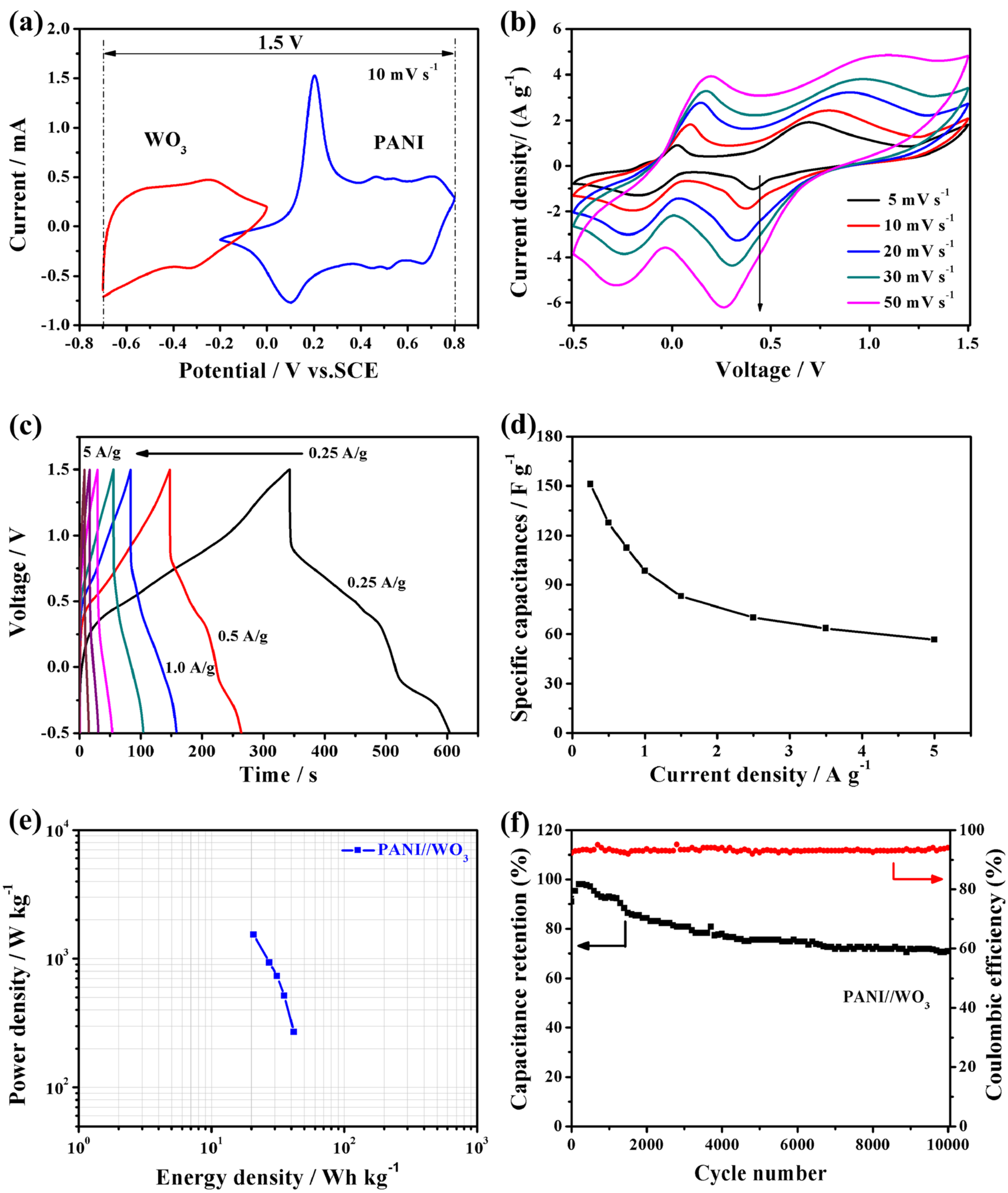

Fig. 4 **a** Comparative CV curves of PANI and WO_3 electrodes performed in three electrode cell in 1 M H_2SO_4 electrolyte at a scan rate of 10 mV s^{-1}; **b** CV curves an PANI//WO_3 ASCs at different scan rates in 1 M H_2SO_4 electrolyte; **c** galvanostatic charge/discharge curves of PANI//WO_3 ASCs at different current densities; **d** specific capacitance of the ASCs at different current densities; **e** Ragone plot related to energy and power densities of the PANI//WO_3 ASCs in comparison to asymmetric supercapacitor recently reported in the literature; **f** cycling stability of the PANI//WO_3 ASCs test at current density of 5 A g^{-1}

nonlinearity in the charge and discharge curves indicates some contribution of the redox reaction from PANI and WO_3, which is in agreement with the result of the CV curves. According to the formula of specific capacitance, the gravimetric capacitance of PANI//WO_3 ASCs as high as 151 F g^{-1} at a current density of 0.25 A g^{-1} (Fig. 4d), which is attributed to the combination of high specific capacitances in both electrodes.

Figure 4e shows Ragone plot for energy density and power density. The energy and power densities are calculated from the discharge curves at different current densities. The PANI//WO_3 ASCs with a cell voltage of 2.0 V can exhibit an energy density of 41.9 Wh kg^{-1} at a power density of 261 W kg^{-1} and remained 20.8 Wh kg^{-1} at 1631 W kg^{-1}. The PANI//WO_3 ASCs also exhibit much

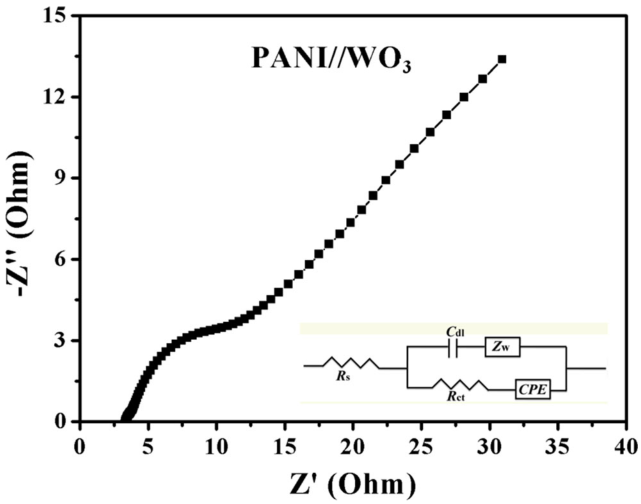

Fig. 5 Nyquist plots of PANI//WO_3 asymmetric supercapacitors for two-electrode system (the *inset* of modeled equivalent circuit of electrochemical impedance spectroscopy)

higher energy density than other reported ASCs, such as RGO-RuO_2//RGO-PANI (26.3 Wh kg^{-1}) [13], MnO_2//FeOOH (24.0 Wh kg^{-1}) [14], $NiCo_2O_4$@MnO_2//activated carbon (35.0 Wh kg^{-1}) [35]. The high energy density of PANI//WO_3 ASCs is attributed to the enlarged operation voltage and the high specific capacitance of both electrodes.

The long-term cycling stability is an important criterion for supercapacitor applications. The cycling endurance measurement over 10,000 cycles for PANI//WO_3 ASCs was conducted using galvonostatic charge/discharge test at 5 A g^{-1} between −0.5 and 1.5 V (Fig. 4f). It can be seen that the asymmetric cell exhibits excellent cycling stability with 71 % capacitance of its initial value after 10,000 cycles.

Figure 5 shows Nyquist plot of PANI//WO_3 ASCs with the semicircle in the high-frequency region and the greater than 45° sloped curve in the low-frequency region, in which results indicate a low charge-transfer resistance in the electrochemical system and a pronounced capacitive behavior with small diffusion resistance, respectively [36]. The impedance spectra were analyzed by the software of ZSimpWin on the basis of the electrical equivalent circuit (the inset of Fig. 5), the diameter of the semicircle corresponds to the charge-transfer resistance (R_{ct}) caused by Faradic reactions and EDLC (C_{dl}) at the electrode/electrolyte interface. The 45° sloped portion in the mediate-frequency region, known as Warburg resistance (Z_w), is a result of the frequency dependence of electrolyte diffusion/transport into the porous electrodes [37]. *CPE* is the constant phase element [8]. In the high-frequency region, PANI//WO_3 ASCs exhibit an R_S value of 3.346 Ω, indicating the lower charge-transfer resistance and an excellent electronic conductivity.

Conclusions

In summary, a high energy density asymmetric supercapacitor (PANI//WO_3) is assembled using polyaniline (PANI) nanotubes as the positive electrode and WO_3 rods as the negative electrode in 1 M H_2SO_4 aqueous electrolyte. The novel asymmetric supercapacitor (PANI//WO_3) device operates with a voltage of 2.0 V and achieved a remarkable energy density of 41.9 Wh kg^{-1} at a power density of 261 W kg^{-1}. Furthermore, the device showed an excellent charge/discharge cycling performance, with capacitance retention of 71 % after 10,000 cycles. The cheap conductive polymers and metal oxide electrode materials and cell assembly strategy of the ASC provide a promising research direction for the next generation and low-cost supercapacitor with high energy density storage demands.

References

1. Wang GP, Zhang L, Zhang JJ (2012) A review of electrode materials for electrochemical supercapacitors. Chem Soc Rev 41:797–828
2. Padmanathan N, Selladurai S (2014) Electrochemical capacitance of porous NiO–CeO_2 binary oxide synthesized via sol–gel technique for supercapacitor. Ionics 20:409–420
3. Wang HL, Xu ZW, Li Z, Cui K, Ding J, Kohandehghan A, Tan XH, Zahiri B, Olsen BC, Holt CMB, Mitlin D (2014) Hybrid device employing three-dimensional arrays of MnO in carbon nanosheets bridges battery-supercapacitor divide. Nano Lett 14:1987–1994
4. Xu J, Wang QF, Wang XW, Xiang QY, Liang B, Chen D, Shen GZ (2013) Flexible asymmetric supercapacitors based upon Co_9S_8 nanorod//Co_3O_4@RuO_2 nanosheet arrays on carbon cloth. ACS Nano 7:5453–5462
5. Wang YG, Li HQ, He P, Hosono E, Zhou HS (2010) Nano active materials for lithium-ion batteries. Nanoscale 2:1294–1305
6. Liang YR, Liang FX, Zhong H, Li ZH, Fu RW, Wu DC (2013) An advanced carbonaceous porous network for high-performance organic electrolyte supercapacitors. J Mater Chem A 1:7000–7005
7. Wang FX, Xiao SY, Hou YY, Hu CL, Liu LL, Wu YP (2013) Electrode materials for aqueous asymmetric supercapacitors. RSC Adv 3:13059–13084
8. Chang J, Jin MH, Yao F, Kim TH, Le VT, Yue HY, Gunes F, Li B, Ghosh A, Xie SS, Lee YH (2013) Asymmetric supercapacitors based on graphene/MnO_2 nanospheres and graphene/MoO_3 nanosheets with high energy density. Adv Funct Mater 23:5074–5083
9. Gao HC, Xiao F, Ching CB, Duan HW (2012) High-performance asymmetric supercapacitor based on graphene hydrogel and nanostructured MnO_2. ACS Appl Mater Interfaces 4:2801–2810
10. Tang W, Liu LL, Tian S, Li L, Yue YB, Wu YP, Zhu K (2011) Aqueous supercapacitors of high energy density based on MoO_3 nanoplates as anode material. Chem Commun 47:10058–10060
11. Zhou C, Zhang YW, Li YY, Liu JP (2013) Construction of high-capacitance 3D CoO@ polypyrrole nanowire array electrode for aqueous asymmetric supercapacitor. Nano Lett 13:2078–2085
12. Huang JC, Xu PP, Cao DX, Zhou XB, Yang SN, Li YJ, Wang GL (2014) Asymmetric supercapacitors based on β-Ni$(OH)_2$ nanosheets and activated carbon with high energy density. J Power Sources 246:371–376

13. Zhang JT, Jiang JW, Li HL, Zhao XS (2011) A high-performance asymmetric supercapacitor fabricated with graphene-based electrodes. Energy Environ Sci 4:4009–4015
14. Jin WH, Cao GT, Sun JY (2008) Hybrid supercapacitor based on MnO_2 and columned FeOOH using Li_2SO_4 electrolyte solution. J Power Sources 175:686–691
15. Zou BX, Liang Y, Liu XX, Diamond D, Lau KL (2011) Electrodeposition and pseudocapacitive properties of tungsten oxide/polyaniline composite. J Power Sources 196:4842–4848
16. Xiao X, Ding TP, Yuan LY, Shen YQ, Zhong QZ, Zhang XH, Cao YZ, Hu B, Zhai T, Gong L, Chen J, Tong YX, Zhou J, Wang ZL (2012) WO_{3-x}/MoO_{3-x} core/shell nanowires on carbon fabric as an anode for all-solid-state asymmetric supercapacitors. Adv Energy Mater 2:1328–1332
17. Snook GA, Kao P, Best AS (2011) Conducting-polymer-based supercapacitor devices and electrodes. J Power Sources 196:1–12
18. Li XG, Li A, Huang MR (2008) Facile high-yield synthesis of polyaniline nanosticks with intrinsic stability and electrical conductivity. Chem Eur J 14:10309–10317
19. Li XG, Lü QF, Huang MR (2008) Self-stabilized nanoparticles of intrinsically conducting copolymers from 5-sulfonic-2-anisidine. Small 4:1201–1209
20. Li XG, Feng H, Huang MR (2009) Strong adsorbability of mercury ions on aniline/sulfoanisidine copolymer nanosorbents. Chem Eur J 15:4573–4581
21. Aricò AS, Bruce P, Scrosati B, Tarascon JM, Schalkwijk WV (2005) Nanostructured materials for advanced energy conversion and storage devices. Nat Mater 4:366–377
22. Liang RL, Cao HQ, Qian D (2011) MoO_3 nanowires as electrochemical pseudocapacitor materials. Chem Commun 47:10305–10307
23. Hechavarría L, Hu H, Miranda M, Nicho ME (2009) Electrochromic responses of low-temperature-annealed tungsten oxide thin films in contact with a liquid and a polymeric gel electrolyte. J Solid State Electrochem 13:687–695
24. Lu XH, Zhai T, Zhang XH, Shen YQ, Yuan LY, Hu B, Gong L, Chen J, Gao YH, Zhou J, Tong YX, Wang ZL (2012) WO_{3-x}@Au@MnO_2 core–shell nanowires on carbon fabric for high-performance flexible supercapacitors. Adv Mater 24:938–944
25. Xue XY, He B, Yuan S, Xing LL, Chen ZH, Ma CH (2011) SnO_2/WO_3 core–shell rods and their high reversible capacity as lithium-ion battery anodes. Nanotechnology 22:395702
26. Mu JJ, Ma GF, Peng H, Li JJ, Sun KJ, Lei ZQ (2013) Facile fabrication of self-assembled polyaniline nanotubes doped with d-tartaric acid for high-performance supercapacitors. J Power Sources 242:797–802
27. Pouget JP, Jozefowicz ME, Epstein AJ, Tang X, MacDiarmid AG (1991) X-ray structure of polyaniline. Macromolecules 24:779–789
28. Li XG, Feng H, Huang MR (2010) Redox sorption and recovery of silver ions as silver nanocrystals on poly(aniline-co-5-sulfo-2-anisidine) nanosorbents. Chem Eur J 16:10113–10123
29. Li J, Liu XH, Han QF, Yao XX, Wang X (2013) Formation of WO_3 nanotube-based bundles directed by $NaHSO_4$ and its application in water treatment. J Mater Chem A 1:1246–1253
30. Huo NJ, Yang SX, Wei ZM, Li JB (2013) Synthesis of WO_3 nanostructures and their ultraviolet photoresponse properties. J Mater Chem C 1:3999–4007
31. Stilwell DE, Park SM (1988) Electrochemistry of conductive polymers II. Electrochemical studies on growth properties of polyaniline. J Electrochem Soc 135:2254–2262
32. Zheng HD, Ou JZ, Strano MS, Kaner RB, Mitchell A, Kalantar-zadeh K (2011) Nanostructured tungsten oxide–properties, synthesis, and applications. Adv Funct Mater 21:2175–2196
33. Gu ZJ, Ma Y, Yang WS, Zhang GJ, Yao JN (2005) Self-assembly of highly oriented one-dimensional h-WO_3 nanostructures. Chem Commun 28:3597–3599
34. Fan ZJ, Yan J, Wei T, Zhi LJ, Ning GQ, Li TY, Wei F (2011) Asymmetric supercapacitors based on graphene/MnO_2 and activated carbon nanofiber electrodes with high power and energy density. Adv Funct Mater 21:2366–2375
35. Xu KB, Li WY, Liu Q, Li B, Liu XJ, An L, Chen ZQ, Zou RJ, Hu JQ (2014) Hierarchical mesoporous $NiCo_2O_4$@MnO_2 core–shell nanowire arrays on nickel foam for aqueous asymmetric supercapacitors. J Mater Chem A 2:4795–4802
36. Wang JG, Yang Y, Huang ZH, Kang FY (2013) A high-performance asymmetric supercapacitor based on carbon and carbon–MnO_2 nanofiber electrodes. Carbon 61:190–199
37. Cheng Q, Tang J, Ma J, Zhang H, Shinya N, Qin LC (2011) Graphene and nanostructured MnO_2 composite electrodes for supercapacitors. Carbon 49:2917–2925